MCB
Journals.ASM.org

Activation of Myeloid Cell-Specific Adhesion Class G Protein-Coupled Receptor EMR2 via Ligation-Induced Translocation and Interaction of Receptor Subunits in Lipid Raft Microdomains

Yi-Shu Huang,[a] Nien-Yi Chiang,[a] Ching-Hsun Hu,[a] Cheng-Chih Hsiao,[b] Kai-Fong Cheng,[a] Wen-Pin Tsai,[c] Simon Yona,[d] Martin Stacey,[e] Siamon Gordon,[f] Gin-Wen Chang,[b] and Hsi-Hsien Lin[a,b]

Graduate Institute of Biomedical Sciences[a] and Department of Microbiology and Immunology, College of Medicine,[b] Chang Gung University, Kwei-San, Tao-Yuan, Taiwan; Division of Rheumatology, Allergy, and Immunology, Chang Gung Memorial Hospital at Keelung, Keelung, Taiwan[c]; Department of Immunology, The Weizmann Institute of Science, Rehovot, Israel[d]; Institute of and Molecular and Cellular Biology, University of Leeds, Leeds, United Kingdom[e]; and Sir William Dunn School of Pathology, University of Oxford, Oxford, United Kingdom[f]

The adhesion class G protein-coupled receptors (adhesion-GPCRs) play important roles in diverse biological processes ranging from immunoregulation to tissue polarity, angiogenesis, and brain development. These receptors are uniquely modified by self-catalytic cleavage at a highly conserved GPCR proteolysis site (GPS) dissecting the receptor into an extracellular subunit (α) and a seven-pass transmembrane subunit (β) with cellular adhesion and signaling functions, respectively. Using the myeloid cell-restricted EMR2 receptor as a paradigm, we exam the mechanistic relevance of the subunit interaction and demonstrate a critical role for GPS autoproteolysis in mediating receptor signaling and cell activation. Interestingly, two distinct receptor complexes are identified as a result of GPS proteolysis: one consisting of a noncovalent α-β heterodimer and the other comprising two completely independent receptor subunits which distribute differentially in membrane raft microdomains. Finally, we show that receptor ligation induces subunit translocation and colocalization within lipid rafts, leading to receptor signaling and inflammatory cytokine production by macrophages. Our present data resolve earlier conflicting results and provide a new mechanism of receptor signaling, as well as providing a paradigm for signal transduction within the adhesion-GPCR family.

The adhesion-class G protein-coupled receptors (adhesion-GPCRs) constitute the second largest GPCR subfamily, whose 33 members are expressed restrictedly in cells of the central nervous, immune, and/or reproductive systems (2, 53). Adhesion-GPCRs are uniquely characterized by the chimeric composition of a large extracellular domain (ECD) and a seven-pass transmembrane (7TM) region. While the 7TM region is predicted to transduce cellular signals, the ECD of adhesion-GPCRs contains multiple repeats of protein modules such as the lectin-like, immunoglobulin (Ig)-like, epidermal growth factor (EGF)-like, and cadherin-like motifs known to mediate protein-protein interaction (2, 53). Adhesion-GPCRs are thus thought to possess a dual cellular adhesion and signaling function. Recent studies have revealed many important functions for adhesion-GPCRs: these include development of the brain frontal cortex (34), circulation of cerebrospinal fluid (44), central nervous system (CNS)-restricted angiogenesis and vascularization (1, 10, 21), myelination of Schwann cells (30, 31), Usher syndrome (29, 49), cellular polarity (16, 23), epididymal fluid regulation and male fertility (4, 12), and immune recognition and regulation (11, 18, 27, 47), as well as tumor growth and metastasis (8, 17, 43, 50). However, the molecular mechanisms mediating the biological functions of adhesion-GPCRs remain to be fully characterized.

In addition to the large mosaic ECD, the complex pre- and posttranslational modifications that produce multiple receptor isoforms and the lack of defined ligands also present a great challenge in deciphering the molecular mechanisms of adhesion-GPCRs. Of note is the conserved proteolytic modification at the GPCR proteolysis site (GPS) proximal to the 7TM region (26, 28). As a result of GPS proteolysis, most adhesion-GPCRs are cleaved into two polypeptide chains with distinct structural and functional features: cellular adhesive ECD (α-) and signaling 7TM (β-) receptor subunits, respectively (28, 53).

GPS proteolysis occurs in a highly conserved Cys-rich GPS motif that is found almost exclusively in adhesion-GPCRs (28, 53). Intriguingly, the cleaved α-subunit stays firmly on the plasma membrane rather than being shed from the cell surface. Moreover, our previous analysis of EGF-like module-containing mucin-like hormone receptor-like 2 (EMR2) has revealed that GPS proteolysis is mediated via a self-catalytic reaction reminiscent of the one utilized by N-terminal nucleophile (Ntn)-hydrolases and hedgehog (Hh) proteins (26). Thus, GPS autoproteolysis is likely an inherent process important for the functional maturation of most adhesion-GPCRs. Indeed, GPS proteolysis was found to be required for the efficient surface trafficking of a number of adhesion-GPCRs (28). Furthermore, point mutations affecting GPS proteolysis of certain receptors are linked to human genetic disorders (34, 37). Nevertheless, how the functions of adhesion-GPCRs are mediated by the two receptor subunits is unknown.

It is commonly accepted that the α-subunit remains mem-

Received 10 November 2011 Returned for modification 9 December 2011
Accepted 25 January 2012
Published ahead of print 6 February 2012
Address correspondence to Gin-Wen Chang, ginwenchang@gmail.com, or Hsi-Hsien Lin, hhlin@mail.cgu.edu.tw.
Y.-S.H. and H.-H.L. contributed equally to this article.

doi:10.1128/MCB.06557-11

brane bound via a tight but noncovalent interaction with the β-subunit. Several lines of evidence strongly support this conclusion. First, the α-subunit can be readily immunoprecipitated (IP) by antibodies specific to the 7TM β-subunit (20, 22). Second, soluble fusion proteins containing the α-subunit and a tag such as the Ig-Fc region were cleaved normally and affinity purified efficiently (3, 26). However, recent studies on the latrophilin 1 receptor has challenged this belief (40, 48) and suggested an intriguing alternative that the cleaved latrophilin α-subunit can anchor itself on the membrane independently. Specifically, it was found that the two latrophilin subunits are solubilized differentially by perfluoro-octanoic acid (PFO) and can be internalized independently. Upon antibody cross-linking, both subunits formed distinct patches and displayed different lateral diffusion rates on the cell surface. Cross-interaction between complementary subunits of different adhesion-GPCRs is also readily detected. Finally, agonist binding to the α-subunit induces reassociation of the two subunits and provokes signal transduction via the β-subunit (40, 48). On the contrary, Serova et al. claim in a more recent study that the majority of latrophilin subunits in fact form a noncovalent heterodimeric complex, with only a small minority of subunits independently separated (38).

Since the distinct subunit organization models mentioned above would almost certainly lead to different modes of molecular interaction and functional outcomes, we decided to investigate the structural and functional relationship of myeloid cell-restricted EMR2 receptor subunits. Here, we show that EMR2 receptor function depends critically on GPS autoproteolysis, which produces two distinct receptor complexes. One is a heterodimer of noncovalently linked α- and β-subunits, while the other consists of independent α- and β-subunits located at different membrane raft microdomains. Our data further suggest that GPS autoproteolysis is not required for the self-anchoring of EMR2 α-subunit on the plasma membrane. Moreover, ligation of the independent EMR2 α-subunit brings it in close contact with the β-subunit in lipid rafts, inducing proinflammatory cytokine production by human monocytes/macrophages. The generation of two different receptor complexes is thought to provide another level of functional diversity and regulation for adhesion-GPCRs.

MATERIALS AND METHODS

Reagents and antibodies. Unless otherwise specified, general reagents and antibodies were obtained from Sigma-Aldrich (St. Louis, MO). DNA and protein reagents were obtained from Invitrogen (Carlsbad, CA), Qiagen (Valencia, CA), Fermentas (Ontario, Canada), New England Biolabs (Massachusetts), or Amersham (GE Healthcare). The monoclonal antibodies (MAbs) used in the study include EMR2 stalk-specific 2A1 and anti-CD4 (1F6) from AbD Serotec (Kidlington, United Kingdom), anti-c-myc (9E10) from Invitrogen; anti-HA.11 (16B12) from Covance (New Jersey), anti-CD71 (H68.4) from Zymed Laboratories (San Francisco, CA), anti-β-actin (clone C4) and chicken anti-DAF (CD55) polyclonal antibodies from Chemicon (California), and anti-caveolin-1 (7C8) from Upstate (Lake Placid, NY). Fluorochrome-conjugated goat anti-mouse IgG was from Jackson Immunoresearch (West Grove, PA). Mouse IgG1 isotype control (clone 11711) was from R&D Systems (Minnesota). The plasmids containing PAR1 and CD4-HA-AATN cDNAs were kindly provided by Hua-Wen Fu and Shaun R. Coughlin (45) and Min Li (39), respectively.

Cell culture and transient transfection. All cell culture media and supplements, including 10% heat inactivated fetal calf serum (FCS), 2 mM L-glutamine, 50 IU of penicillin/ml, and 50 μg of streptomycin/ml, were purchased from Invitrogen. CHO-K1 and HEK293T cells were cultured in Ham F-12 and Dulbecco modified Eagle medium, respectively. THP-1 cells were cultured in RPMI 1640 and differentiated to macrophage-like cells with 1 μg of phorbol 12-myristate 13-acetate/ml. Baf/3b stable cells were described previously (52). HT1080 stable cells were maintained in minimal essential medium containing 0.3 μg of G418/ml, nonessential amino acids, and 1 mM sodium pyruvate. Transient transfection of expression constructs was performed using Lipofectamine (Invitrogen) reagent as described previously (13). Cells were washed 6 h posttransfection and fed with fresh medium for 2 to 3 days for further analysis.

Construction of expression vectors. All expression vectors were constructed on pcDNA3.1(+)/myc-His vector (Invitrogen) unless otherwise specified. EMR2-mFc, EMR2-WT-myc and EMR2-S518A-myc expression constructs have been described previously (13, 26). The retroviral expression constructs were generated using the pFB-Neo vector system (Stratagene, La Jolla, CA). The HA-EMR4-TM1 construct was made by cloning the ECD and the first TM region of EMR4 into a previously described pSecTaq2A/HA via the HindIII and BamHI sites. Constructs encoding the EMR2-PAR1 chimeric proteins were made by ligating the respective EMR2-ECD cDNA fragments with the full-length PAR1 cDNA using appropriate restriction sites. The EMR2-CD4 chimeric expression constructs were made by cloning the full-length CD4-HA-AATN fragment immediately downstream of the EMR2 stalk via the BamHI and ApaI sites.

Retroviral infection and selection of stable cell lines. HEK293T packaging cells in 10-cm dishes were transfected with 3 μg each of the pFB-Neo expression construct, pVPack-VSV-G, and pVPack-GP vectors (Stratagene) with 25 μl of Lipofectamine in Opti-MEM as recommended by the supplier. Virus-containing supernatant was harvested 48 h posttransfection, to which a final concentration of 5 μg of Polybrene solution/ml was added. HT1080 cells (~40 to 50% confluence) in six-well plates were infected with 1 ml of viral supernatant. Cells were spun for 90 min at 25°C at 600 × *g*, followed by the addition of 2 ml of fresh complete medium 3 h later. The infected cells were then incubated for an additional 24 h at 37°C before selection in medium containing 1 mg of G418/ml. G418-resistant cells were collected after ~2 weeks of selection and confirmed by appropriate analysis.

Preparation of polyclonal antibodies again EMR2 β-subunit. The peptide antigen (Ag), containing 12 amino acid residues (AKADTSKPS TVN) at the C-terminal end of the EMR2 β-subunit, was synthesized and conjugated to the keyhole limpet hemocyanin carrier protein. The Ag was mixed with complete adjuvant and injected subcutaneously into rabbits, followed by injection of the Ag-incomplete adjuvant mixture at the same site 1 month later. The immunized serum was collected periodically to test for its reactivity to the Ag by enzyme-linked immunosorbent assay (ELISA). The polyclonal antiserum was purified first by ammonium sulfate precipitation, followed by use of a Melon Gel IgG spin purification kit (Thermo Scientific, Fremont, CA) according to the standard procedures.

Cell chemotaxis assays. Cell chemotaxis were carried out with a QCM Chemotaxis 96-well cell migration assay kit (Millipore, Bedford, MA). Briefly, the cells were serum starved for ca. 18 to 24 h, detached in phosphate-buffered saline (PBS)–2 mM EDTA, and resuspended at a concentration of 5×10^5 cells/ml in serum-free medium–5% bovine serum albumin (BSA). Cells (100 μl/well) were placed in the upper chamber of a QCM chemotaxis plate equipped with an 8-μm-pore-size membrane. The bottom chambers were filled with culture medium with or without 10% FCS as chemoattractants. The plates were kept in a 37°C incubator for 5 h. Migrated cells were dissociated from the bottom of the filter membrane and stained with CyQuant GR dye. The fluorescence intensity was measured in a fluorescence plate reader (Molecular Devices) with a 480/520-nm filter set.

PFO treatment of EMR2-mFc-Dynabead complex and EMR2-expressing cells. Protein A-conjugated Dynabeads (Dynal A.S., Oslo, Norway) were blocked with 1% BSA in Hanks balanced salt solution for 1 h and then mixed with EMR2-mFc containing conditioned medium for 2 h at 4°C. After extensive washes, beads were precipitated by magnet separa-

tion. The EMR2-mFc-dynabead complexes or cells expressing recombinant EMR2 proteins were incubated for 10 min on ice in perfluorooctanoic acid (PFO)-containing PBS buffer (PFO solution). The supernatant was collected following centrifugation at 13,000 rpm at 4°C for 15 min, and the pellet was dissolved in radioimmunoprecipitation assay lysis buffer to obtain total cell lysate.

Flow cytometry analysis. Transiently transfected cells were harvested and fixed in 2% paraformaldehyde-PBS at 4°C for 30 min. The cells were then blocked for 1 h in ice-cold blocking buffer (1% BSA, 5% serum of secondary antibody, and PBS) with or without 0.1% saponin. Then, the cells were incubated with the indicated primary antibody diluted in blocking buffer for 1 h before washing. The cells were incubated for 1 h with fluorochrome-conjugated second antibody in blocking buffer (1:200) and then washed three times by cold PBS and subjected to analysis by using a FACScan flow cytometer (BD Biosciences).

Antibody patching. Transiently transfected cells cultured on coverslips (BD BioCoat poly-D-lysine; BD Biosciences) were blocked for 1 h in ice-cold blocking buffer (1% BSA, 5% normal serum of secondary antibody, and PBS). The cells were incubated with 2A1 MAb (5 μg/ml) for 30 min, followed by Alexa Fluor 647-conjugated anti-mouse IgG (1:200; Invitrogen) for 30 min on ice, with extensive washes in between by ice-cold blocking buffer. The cells were then transferred to a 22°C incubator for 15 min for patching and immediately fixed in 2% paraformaldehyde-PBS at 4°C before washing. For lipid raft patching, the cells were incubated sequentially with Alexa Fluor 647-conjugated cholera toxin β-subunit (10 μg/ml) and anti-cholera toxin β-subunit polyclonal antibodies (1:200; Invitrogen) for 30 min each on ice with extensive washes in between. The cells were then transferred to a 22°C incubator for 15 min for patching and immediately fixed in 2% paraformaldehyde-PBS at 4°C for 20 min. The fixed cells were then processed for 2A1 staining (5 μg/ml) in cold blocking buffer (PBS, 1% BSA, and 5% normal serum from a secondary antibody-producing host animal) using Alexa Fluor 488-conjugated anti-mouse IgG (1:200; Invitrogen). Coverslips were mounted onto slides with antifade mounting medium (ProLong Gold Antifade reagent with DAPI 4′,6′-diamidino-2-phenylindole [Invitrogen]). Fluorescence images were taken at 1,000-fold magnification using a confocal microscope (Zeiss LSM 510 Meta).

Immunoprecipitation. Anti-myc antibody-conjugated (100 μl) agarose beads were washed twice with 500 μl of PBS and then incubated with 250 μl of blocking buffer (1% BSA in PBS) for 3 h at 4°C. Total cell lysates (~150 μg) were precleared by incubating with unconjugated agarose beads, spun, and then mixed gently with the conjugated agarose beads overnight at 4°C with end-over-end rotation. After incubation, agarose beads were pelleted by centrifugation at 1,000 × g for 3 min at 4°C and washed five times each with 250 μl of blocking buffer. Finally, equal volume of 2× sodium dodecyl sulfate loading dye was added for subsequent Western blotting.

Lipid raft floatation. All lipid raft separation procedures were carried out on ice. Cells (~5×10^6 cells) were washed three times with ice-cold PBS and then lysed in 150 μl of TNET buffer (25 mM Tris-HCl [pH 7.5], 150 mM NaCl, 5 mM EDTA, 1 mM EGTA, 1% Triton X-100, 10 mM NaF, 1 mM sodium pyrophosphate, 1 mM Na_3VO_4, 1× protease inhibitor cocktail) for 30 min. Total cell lysates were passed through a 30-gauge needle 20 times on ice and then centrifuged at 1,000 × *g* for 10 min at 4°C to collect the supernatant for protein quantification. Typically, 200 μl of cell lysate (~500 μg of protein) was mixed with 400 μl of 60% Opti-Prep and then placed at the bottom of a 5-ml polyallomer ultracentrifuge tube (Beckman). The samples were overlaid sequentially with 3,400 μl of 30% and 200 μl of 5% ice-cold Opti-Prep medium diluted in TNET buffer and subjected to ultracentrifugation at 200,000 × *g* for 16 h at 4°C. After ultracentrifugation, seven equal fractions (~600 μl/fraction) were collected from the top of the tube for Western blotting.

Thrombin treatment and cell surface protein biotinylation and immunoprecipitation. Transfected cells were lifted from the plates, washed, and divided equally into two 1.5-ml Eppendorf tubes. The cells were incubated in ~500 μl of thrombin digestion solution (10 mM HEPES–Opti-MEM) in the presence or absence of thrombin (200 nM, 23.5 U) for 30 min at 37°C before the supernatants were collected. The cells were subjected to fluorescence-activated cell sorting (FACS) analysis or cell lysis for Western blot analysis. For cell surface protein biotinylation, thrombin-treated cells were washed three times with PBS (pH 8.0). The cells were suspended in 820 μl of PBS (pH 8.0) at a concentration of ~2.5×10^6 cells/ml and mixed with 180 μl of ~10 mM biotin solution to a final concentration of ~2 mM. After incubation at room temperature for 30 min by end-over-end rotation, the reaction was stopped by washing the cells in 100 mM glycine solution for three times to quench and remove the excess biotin reagent. Cells were lysed in ice-cold TNET lysis buffer to collect cell lysate for immunoprecipitation using streptavidin-coated agarose beads.

Detection of cytokines by ELISA. THP-1 cells or primary monocytes isolated from peripheral blood mononuclear cells were resuspended in RPMI complete medium at 1×10^6 or 3×10^4 cells/ml in the absence or presence of lipopolysaccharide (LPS). The cells (1 ml/well) were stimulated with soluble or immobilized 2A1 (precoated on plates) or IgG1 isotype control antibody in six-well plates for 24 h. For the lipid raft depletion experiments, the cells were pretreated with lovastatin (5 or 10 μM) for 12 h or filipin (0.1 μg/ml) for 30 min in serum-free RPMI medium. The cells were then spun and resuspended in serum-free RPMI medium with lovastatin (5 or 10 μM) or filipin (1 ng/ml) and stimulated with immobilized 2A1 or IgG1 isotype control antibody in six-well plates. The supernatant was collected and spun, and the concentration of the cytokines was determined by using a DuoSet ELISA development kit (R&D Systems, Minnesota) according to the manufacturer's protocol.

Statistical analysis. Quantifications were based on at least three independent experiments. The data are shown as means ± the standard errors of the mean (SEM). Statistical analysis of data was performed by using the Student *t* test using Prism 5 software. The *P* values are indicated by asterisks in the figures.

RESULTS

GPS autoproteolysis is critical for EMR2-mediated cell migration. A role for EMR2 in promoting cell migration was demonstrated previously (52). To investigate the functional involvement of GPS autoproteolysis in EMR2 receptor, we generated and compared the migratory ability of HT1080 cells stably expressing EMR2-WT, -S518A, or -TM1 receptor. The EMR2-S518A molecule represents the cleavage-deficient receptor whose GPS cleavage site was mutated to Ala, whereas EMR2-TM1 contains only the first TM domain (Fig. 1A). All stable cell lines show similar growth characteristics and express comparable levels of EMR2, as examined by flow cytometric and Western blotting (WB) analysis (Fig. 1B and C).

In agreement with the earlier results, cells expressing EMR2-WT are found to migrate much faster than the vector-only control and EMR2-TM1-expressing cells (Fig. 1D). Interestingly, EMR2-S518A stable cells also migrate slower than do EMR2-WT cells. This result is further confirmed using murine B-lymphoblast Baf/3b stable cell lines. Again, EMR2-WT-expressing cells show an enhanced migration toward CXCL12 than do control and EMR2-S518A stable cells (Fig. 1E). These data indicate that, in addition to the 7TM domain, GPS proteolytic modification is also critical for the cellular function of EMR2.

The extracellular α-subunit of EMR2 can independently self-anchor on the cell membrane. Intrigued by the conflicting findings in the latrophilin 1 receptor and to provide a mechanistic insight into how GPS proteolysis modulates EMR2 function, we examined the ability of EMR2 α-subunit to self-anchor on the plasma membrane. EMR2-expressing cells and precipitated

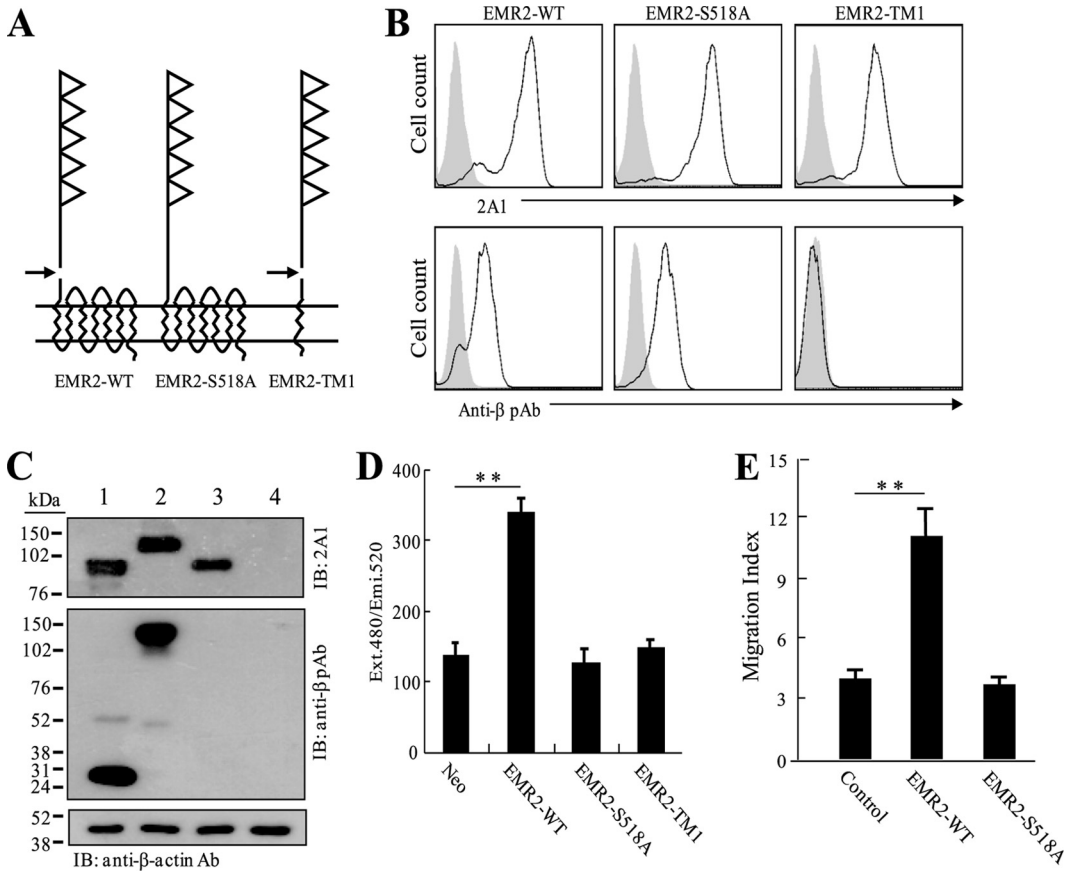

FIG 1 GPS autoproteolysis is critical for EMR2-mediated cell migration. (A) Schematic representation of genetically engineered EMR2 proteins, including the wild-type (EMR2-WT), GPS cleavage-deficient (EMR2-S518A), and TM-truncated (EMR2-TM1) receptors. The GPS cleavage site is indicated by an arrow. (B and C) Flow cytometry (B) and WB analyses (C) confirm the expression of various EMR2 molecules in stable HT1080 cells, using 2A1 MAb and rabbit antiserum specific for the α-subunit and the β-subunit, respectively. Cell lysate from cells expressing EMR2-WT (lane 1), EMR2-S518A (lane 2), and EMR2-TM1 (lane 3) and vector-only control (lane 4) were analyzed. (D and E) Cell migration analysis of stable HT1080 (D) and Baf/3b (E) cells. The data are means ± the SEM of three independent experiments performed in triplicate. **, $P < 0.01$.

EMR2-mFc fusion proteins were treated with PFO, a weak surfactant that does not destroy protein-protein interaction (Fig. 2A). As shown in Fig. 2B, GPS-cleaved EMR2 α-subunit and mFc fragments remain associated even when treated with 1% PFO. However, the α-subunit of EMR2-WT-myc is dissociated efficiently from cell membrane by 0.2% PFO with no apparent effect on the β-subunit (Fig. 2C). Only at 1% PFO is the cell membrane damaged to solubilize α- and β-subunits simultaneously. Similarly, the control EMR2-S518A-myc is detected in the supernatant only after 1% PFO treatment (Fig. 2C). Finally, the α-subunit of endogenous EMR2 receptor in macrophage-like THP-1 cells is solubilized effectively by 1% PFO, again with no detectable β-subunit (Fig. 2D). These results are consistent with the report by Volynski et al. (48) and further indicate that α- and β-subunits associate tightly in soluble EMR2-mFc, but a proportion of the two subunits are separate on the cell membrane. This conclusion was reinforced by the subsequent antibody cross-linking experiment (Fig. 2E). While the α- and β-subunits of EMR2-WT-CFP in control cells show relatively homogeneous distribution on cell membrane, surface cross-linking of the α-subunit by 2A1 MAb produces distinct patches that do not fully overlap with the β-subunit. In contrast, colocalization of both tags is always found in cleavage-deficient EMR2-S518A-CFP before and after antibody cross-linking (Fig. 2E). These data indicate that EMR2 α-subunit is indeed able to self-anchor on the membrane.

If adhesion-GPCR subunits are independent molecular entities on the plasma membrane, one would expect the possibility of cross-interaction between the complementary subunits of different adhesion-GPCR molecules. Indeed, coimmunoprecipitation (co-IP) of complementary subunits has been demonstrated previously between latrophilin 1 and EMR2, as well as GPR56 (40). Additional co-IP experiments using EMR2-WT-myc and HA-EMR4-TM1 show that EMR4 α-subunit is readily co-IP with the EMR2 β-subunit from cells cotransfected with EMR2-WT-myc and HA-EMR4-TM1 constructs, but not those transfected only with the HA-EMR4-TM1 construct (Fig. 2F). Potential false-positive effects caused by β-subunit oligomerization are ruled out by using mixture of cell lysate from cells transfected singly with EMR2-WT-myc or HA-EMR4-TM1 (Fig. 2F). These data verify that the independent α-subunit can cross-interact with the complementary β-subunit of a different adhesion-GPCR.

GPS autoproteolysis is not required for the self-anchoring of EMR2 α-subunit on the membrane. The GPS autoproteolytic reaction is highly similar to the one identified in Hh proteins (25, 36). Interestingly, the final hydrolytic step of Hh biosynthesis is known to be mediated by cholesterol to form a cholesterol adduct,

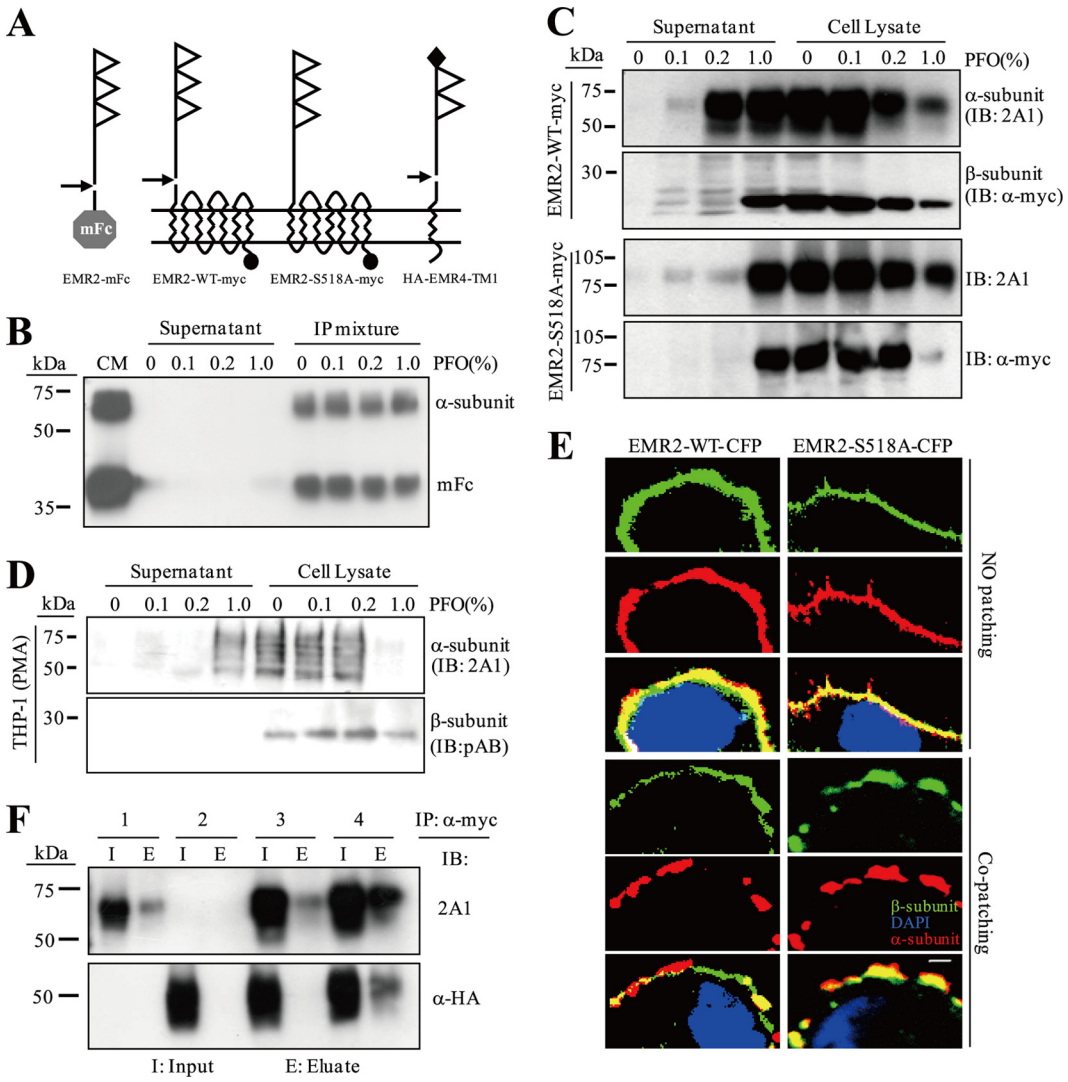

FIG 2 The extracellular α-subunit of EMR2 can independently self-anchor on the cell membrane. (A) Schematic representation of genetically engineered EMR2 and HA-EMR4TM1 proteins analyzed in the assay. The mFc fragment, c-myc and HA tags are represented by a gray hexagon, a small black circle and a diamond, respectively. (B) WB analysis of immunoprecipitated EMR2-mFc treated without (0%) or with PFO (0.1 to 1%). CM, conditioned medium. (C and D) WB analysis of supernatant and total cell lysate of CHO-K1 cells expressing EMR2-WT-myc and EMR2-S518A-myc (C) or macrophage-like THP-1 cells (D) treated without or with PFO (0.1 to 1%). (E) Antibody-patching experiment of CHO-K1 cells. Cells were incubated sequentially with 2A1 and goat anti-mouse IgG–Alexa Fluor 647 antibodies to cluster the α-subunit (red) at 22°C. Cells were counterstained with DAPI to highlight the nucleus (blue). Scale bar, 2 μm. (F) EMR2 receptor subunits can cross-interact with complementary subunits of different adhesion-GPCRs. IP-WB analysis of CHO-K1 cells singly transfected with EMR2-WT-myc (sample 1), HA-EMR4TM1 (sample 2), mixed cell lysate of the two singly transfected cells (sample 3), and cells cotransfected with EMR2-WT-myc and HA-EMR4TM1 (sample 4) was performed. Cell lysate was immunoprecipitated (IP) by anti-myc antibody. I, input; E, eluate.

Hh-Np. This modification allows the otherwise soluble Hh-Np to anchor on the plasma membrane, creating a concentration gradient important for the morphogenic function of Hh (25, 36).

To investigate whether a similar modification occurs during EMR2 maturation, we examined whether GPS autoproteolysis is absolutely required for the membrane association of EMR2 α-subunit. To this end, chimeric EMR2 proteins where the 7TM region of EMR2 is replaced by a protease-activated receptor 1 (PAR1) sequence were generated and analyzed (Fig. 3A). PAR1 is a classical GPCR that can be specifically cleaved and activated by its protease ligand, thrombin (9). We reason that if GPS autoproteolysis is necessary for the membrane association of EMR2 α-subunit, the ECD of GPS cleavage-deficient EMR2-S518A-PAR1 would not associate with the membrane and thrombin treatment should shed it completely from the surface.

Using specific MAbs against the ECD and 7TM region, we show that GPS proteolysis is efficient in EMR2-WT-PAR1 as in WT EMR2 (Fig. 3B). Next, we show the majority of EMR2-S518A-PAR1 is an ~130-kDa uncleaved protein as expected (Fig. 3B, black arrow), even though a background cleavage event is detected (Fig. 3B, black arrowhead). After thrombin digestion, the ~130-kDa band disappears completely (Fig. 3B, asterisk) and two fragments (~70 and ~40 kDa) representing cleaved EMR2-ECD and PAR1 are detected in the supernatant and cell lysate fractions, respectively (Fig. 3B, white arrowhead). In contrast, the same treatment fails to produce additional protein fragments in control

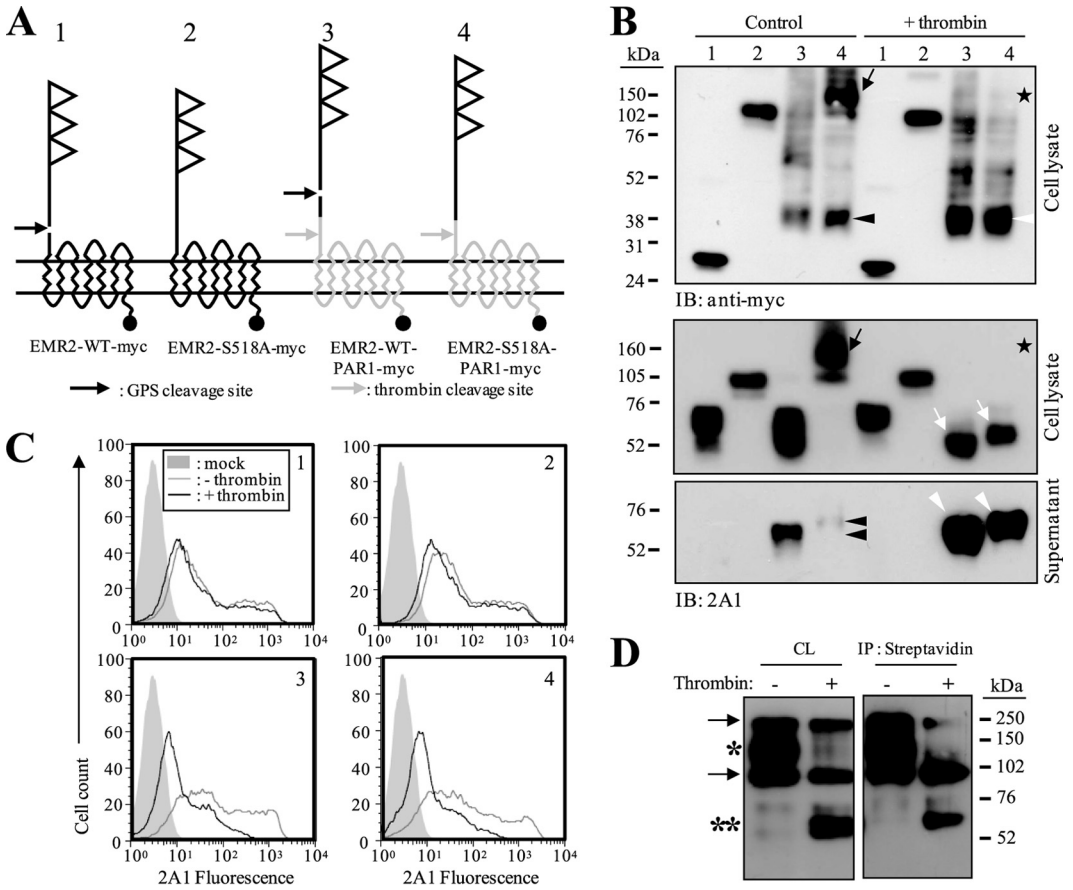

FIG 3 GPS autoproteolysis is not required for the membrane self-anchoring of EMR2 α-subunit. (A) Schematic representation of genetically engineered EMR2 and EMR2-PAR1 chimeric proteins. The PAR1 fragment is represented by a gray zig-zag line, while EMR2 7TM is shown as a black zig-zag line. The GPS and thrombin cleavage sites are indicated by a black and a gray arrow, respectively. (B) WB analysis of H293T cells expressing EMR2-WT-myc (lane 1), EMR2-S518A-myc (lane 2), EMR2-WT-PAR1-myc (lane 3), and EMR2-S518A-PAR1-myc (lane 4) proteins treated with or without thrombin. The ~130-kDa band of EMR2-S518A-PAR1-myc (black arrow) disappears completely after thrombin treatment (asterisk). The resulting fragments are EMR2 α-subunit (~70 kDa, white arrowhead) and the PAR1 fragment (~40 kDa, white arrowhead) in the supernatant and cell lysate fractions, respectively. White arrows indicate the EMR2 α-subunit, while black arrowheads represent the background proteolysis in the EMR2-PAR1 fusion proteins. (C) Flow cytometry analysis of the surface EMR2 expression of the same H293T cells described above treated with or without thrombin. (D) Pulldown WB analysis of EMR2-S518A-PAR1-myc expressing cells. Cells were treated with or without thrombin, subjected to surface biotinylation, and lysed, followed by pulldown (PD) with streptavidin-agarose. Membranes were probed with 2A1 to detect the full-length molecule (*) and cleaved EMR2 α-subunit (**). Arrows indicate nonspecific bands resulting from the biotinylation reaction. CL, total cell lysate.

EMR2-WT and EMR2-S518A samples (Fig. 3B). These results confirm that thrombin digestion is highly specific and efficient.

Unexpectedly, following thrombin digestion an ~60-kDa fully cleaved ECD (α-subunit) is detected in total cell lysate of EMR2-S518A-PAR1-expressing cells (Fig. 3B). Likewise, flow cytometric analysis of the same cells indicates that ~50% of cells stains positive for surface EMR2 after thrombin treatment (Fig. 3C). Again, surface EMR2 levels remain unchanged in cells expressing control EMR2 proteins under the same treatment (Fig. 3C and data not shown). The fact that a substantial fraction of α-subunit remains on the membrane after the complete digestion of EMR2-S518A-PAR1 by thrombin indicates that the membrane association of EMR2 α-subunit does not require GPS proteolysis. To further support this conclusion, EMR2-S518A-PAR1-transfected cells are fully digested by thrombin, surface biotinylated, followed by cell lysis and pulldown (PD) by streptavidin-agarose. WB analysis again shows the presence of a fully cleaved and membrane-bound α-subunit (Fig. 3D).

On the other hand, analysis of EMR2-WT-PAR1 protein shows that a proportion of EMR2 α-subunit seems to interact tightly with the 7TM β-subunit on cell membrane. As such, increased amount of α-subunit was detected in the supernatant of thrombin-treated EMR2-WT-PAR1-transfected cells compared to that of untreated cells (Fig. 3B, lane 3, white arrowhead). Likewise, an ~66% reduction of surface α-subunit was found by flow cytometric analysis in the same cells after thrombin digestion (Fig. 3C and data not shown). Based on these data, we suggest that GPS autoproteolysis leads to the formation of two distinct EMR2 receptor complexes: one is a noncovalently linked α-β heterodimer, and the other consists of independent α- and β-subunits.

EMR2 subunits are differentially distributed on the membrane microdomains. To investigate further the interaction characteristics of the two EMR2 receptor subunits with cell membrane, we decided to analyze their distribution patterns in membrane microdomains. For this purpose, EMR2-CD4 chimeric proteins are engineered in which the entire EMR2-ECD is fused with the

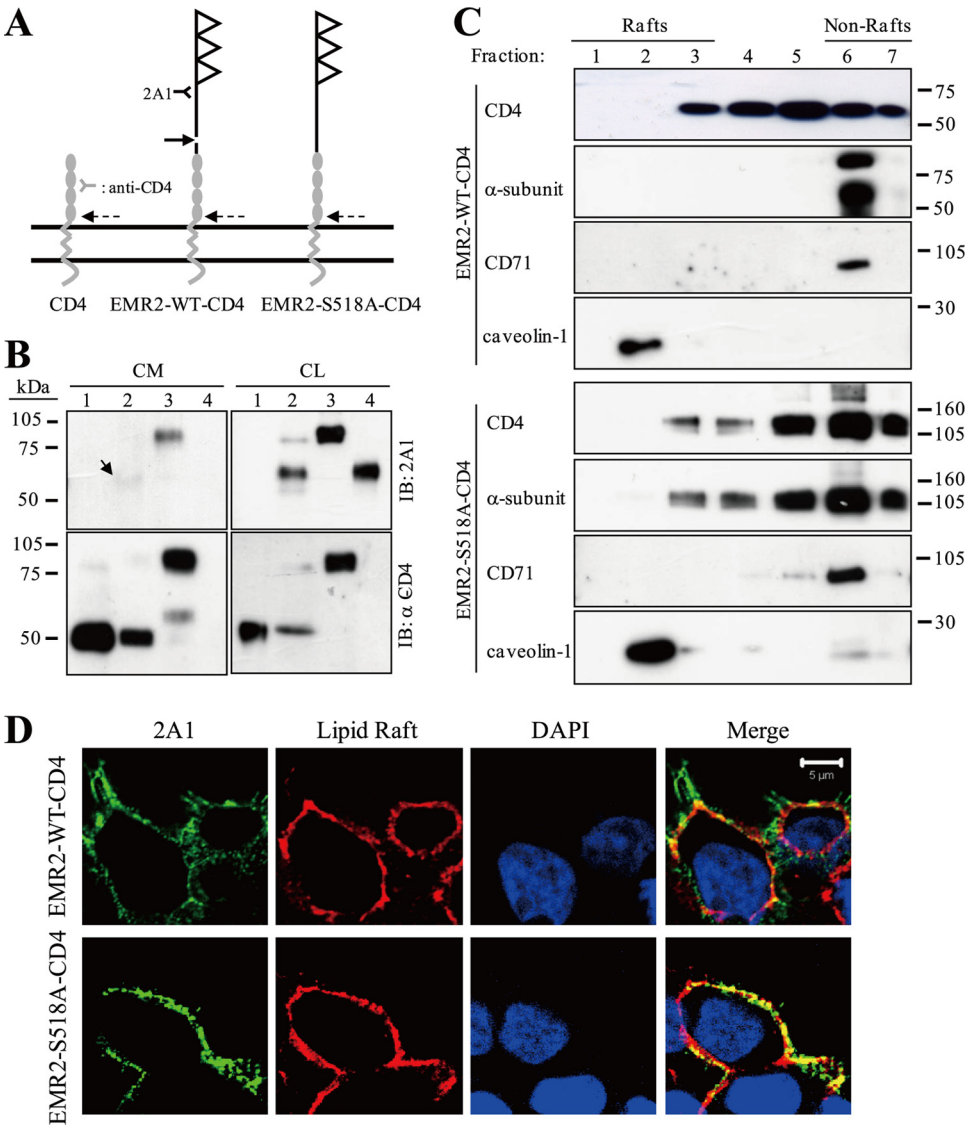

FIG 4 Shedding and differential distribution of receptor subunits of EMR2-CD4 chimeric proteins in membrane raft microdomains. (A) Schematic representation of genetically engineered EMR2-CD4 chimeric proteins. The GPS and CD4 shedding sites are represented by a black arrow and a dash arrow, respectively. (B) WB analysis of the conditioned medium (CM) and total cell lysates (CL) of CHO-K1 cells transfected with CD4 (lane 1), EMR2-WT-CD4 (lane 2), EMR2-S518A-CD4 (lane 3), and EMR2-WT-myc (lane 4) expression constructs. Membranes were probed with 2A1 and anti-CD4 MAbs. The arrow indicates the EMR2 α-subunit shed from the membrane. (C) Lipid raft flotation analysis of transfected CHO-K1 cells. Seven equal fractions were collected and probed by WB analysis. Caveolin-1 and CD71 were used as resident protein markers of the lipid raft and non-lipid raft fractions, respectively. (D) Confocal fluorescence staining of EMR2-CD4 chimeric proteins in lipid raft. Lipid rafts (red) are patched and stained with Alexa Fluor 647-conjugated cholera toxin β-subunit followed by anti-cholera toxin β-subunit polyclonal antibodies, while EMR2 α-subunit (green) is stained by 2A1 and nucleus (blue) by DAPI. Scale bar, 5 μm.

full-length CD4 molecule (Fig. 4A). CD4 was used since it is a well-known lipid raft-associated protein that can be partially shed from the membrane (15, 35, 54). As shown in Fig. 4B, EMR2-WT-CD4 is efficiently processed to produce a cleaved α-subunit and a CD4 receptor, proving its suitability for the analysis of α-subunit distribution in membrane microdomains. WB analysis reveals that partial CD4 ectodomain shedding is apparent not only in the wild-type CD4 molecule but also in EMR2-WT-CD4 and EMR2-S518A-CD4 (Fig. 4B). Coshedding of EMR2-ECD with CD4 is detected in both chimeric receptors as expected, but is more obvious in cleavage-deficient EMR2-S518A-CD4 than in EMR2-WT-CD4. This suggests that GPS cleavage-competent EMR2-WT-CD4 probably produces more membrane-associated α-subunit.

Lipid raft flotation analysis confirms the localization of CD4 molecule in the raft as well as nonraft fractions as reported previously (15, 35). Surprisingly, unlike CD4, the α-subunit of EMR2-WT-CD4 is only detected in the nonraft fractions, whereas the noncleavable EMR2-S518A-CD4 is distributed in the raft and nonraft fractions similar to CD4 (Fig. 4C). The differential localization of EMR2 α-subunit and CD4 on membrane microdomains is confirmed alternatively by antibody patching of lipid rafts. Confocal microscopic analysis reveals that while EMR2-S518A-CD4 displays a strong raft-associated pattern, the α-sub-

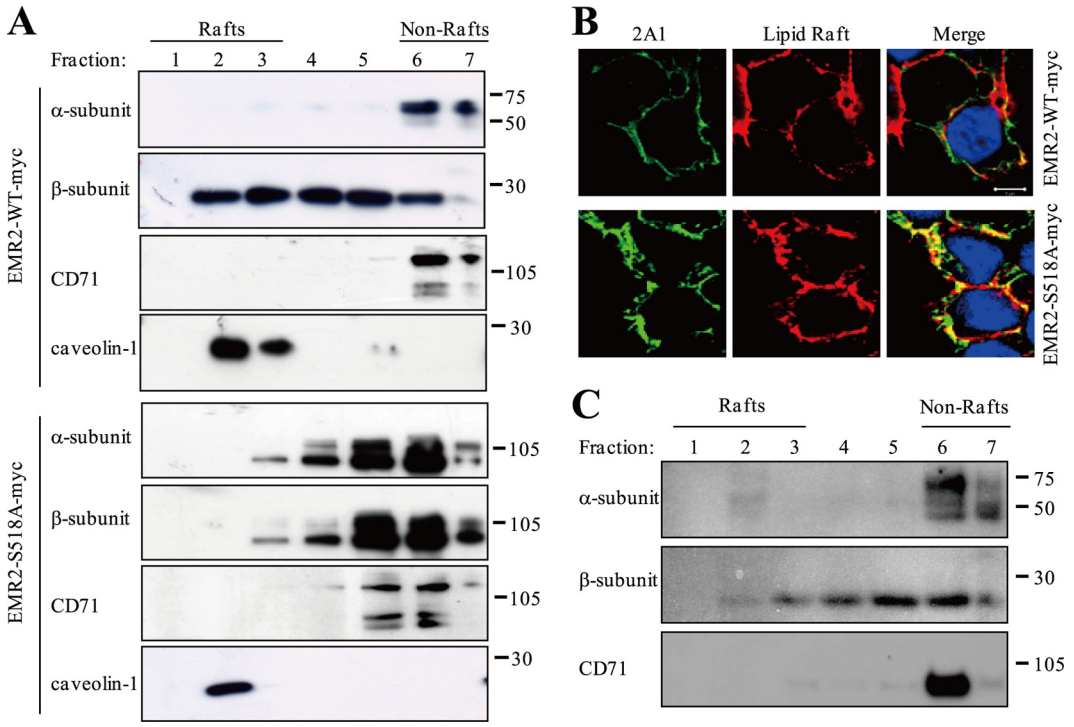

FIG 5 Differential distribution of EMR2 receptor subunits in membrane raft microdomains. (A) Lipid raft flotation analysis of CHO-K1 cells transfected with the EMR2-WT-myc and EMR2-S518A-myc expression constructs. Seven equal fractions were collected and probed by WB analysis. Caveolin-1 and CD71 were used as resident protein markers of the lipid raft and non-lipid raft fractions, respectively. (B) Confocal fluorescence staining of EMR2 proteins in lipid rafts. Lipid rafts (red) of HEK293T cells transfected with the EMR2-WT-myc or EMR2-S518A-myc expression constructs were patched and stained as described in Fig. 4D. EMR2 α-subunit (green) is stained by 2A1 and nucleus (blue) by DAPI. Scale bar, 5 μm. (C) Lipid raft flotation analysis of the endogenous EMR2 protein in macrophage-like THP-1 cells. Seven equal fractions were collected and probed by WB analysis using 2A1 and rabbit anti-EMR2 β-subunit polyclonal antibodies, respectively. CD71 was used as a resident protein marker of the non-lipid raft fractions.

unit of EMR2-WT-CD4 shows only minimal colocalization with lipid rafts (Fig. 4D).

Since an increasing number of GPCRs are known to reside in the raft microdomains (7, 32), the membrane distribution of EMR2-WT-myc and EMR2-S518A-myc was examined. Surprisingly, while the α-subunit is again detected only in the nonraft fractions, EMR2 β-subunit is identified in both the raft and nonraft fractions (Fig. 5A and B). As expected, the distribution of EMR2-S518A-myc is the same as the β-subunit of EMR2-WT-myc. Most importantly, similar differential distribution patterns are identified for endogenous EMR2 α- and β-subunits in THP-1 cells (Fig. 5C) and primary monocytes (data not shown). Altogether, we conclude that the separate EMR2 α- and β-subunits are distributed differentially on membrane raft microdomains, while the noncovalently associated α-β heterodimer is mostly located at the nonraft regions.

Ligation of EMR2 α-subunit induces translocation to lipid rafts, colocalization with the β-subunit and subsequent generation of inflammatory cytokines. We have previously shown that ligation of EMR2 by the α-subunit specific 2A1 MAb strongly potentiates neutrophil responses to inflammatory stimuli, suggesting that 2A1 is likely an EMR2 receptor agonist (5, 52). Is 2A1-induced EMR2 function caused by the interplay between the two separate subunits? We first investigated whether the ligation of α-subunit by 2A1 could modulate its distribution pattern on membrane microdomains. Interestingly, while the α-subunit of control cells stays in the nonraft fractions, the α-subunit of 2A1-treated cells shows a transient migration into the lipid raft fractions (data not shown). 2A1-induced α-subunit translocation to lipid rafts peaks at 2 to 5 min after 2A1 stimulation and gradually returns to its normal distribution pattern. In contrast, the distribution of EMR2 β-subunit shows no obvious changes under the same condition. The same results were obtained in different cell lines, including CHO-K1, HT-1080, and Baf/3b cells (data not shown), suggesting a genuine 2A1-induced effect.

We next investigated the functional consequence of 2A1-induced α-subunit translocation to lipid rafts. For this purpose, THP-1 cells and human primary monocytes were treated with or without 2A1 MAb, followed by the detection of proinflammatory cytokines. Although the myeloid cells responded positively to inflammatory stimuli such as LPS, no cytokine production in 2A1-treated cells was observed (data not shown). Nevertheless, a substantial response was noted in cells incubated with immobilized 2A1 MAb precoated on plates. Under these conditions, immobilized 2A1-induced lipid raft translocation of α-subunit is found to persist for as long as 3 h (Fig. 6A). The same results were obtained in primary monocytes (data not shown). Moreover, the production of proinflammatory cytokines including interleukin-8 (IL-8) and tumor necrosis factor alpha (TNF-α) was readily detected (Fig. 6B and C). Importantly, the effect of immobilized 2A1 on cytokine production is found to be specific in a dose- and time-dependent manner (Fig. 6B, C, and D). As such, no cytokine production is detected when plates are coated with an isotype-control IgG. Furthermore, IL-6 (Fig. 6B and C) and IL-10 (data not

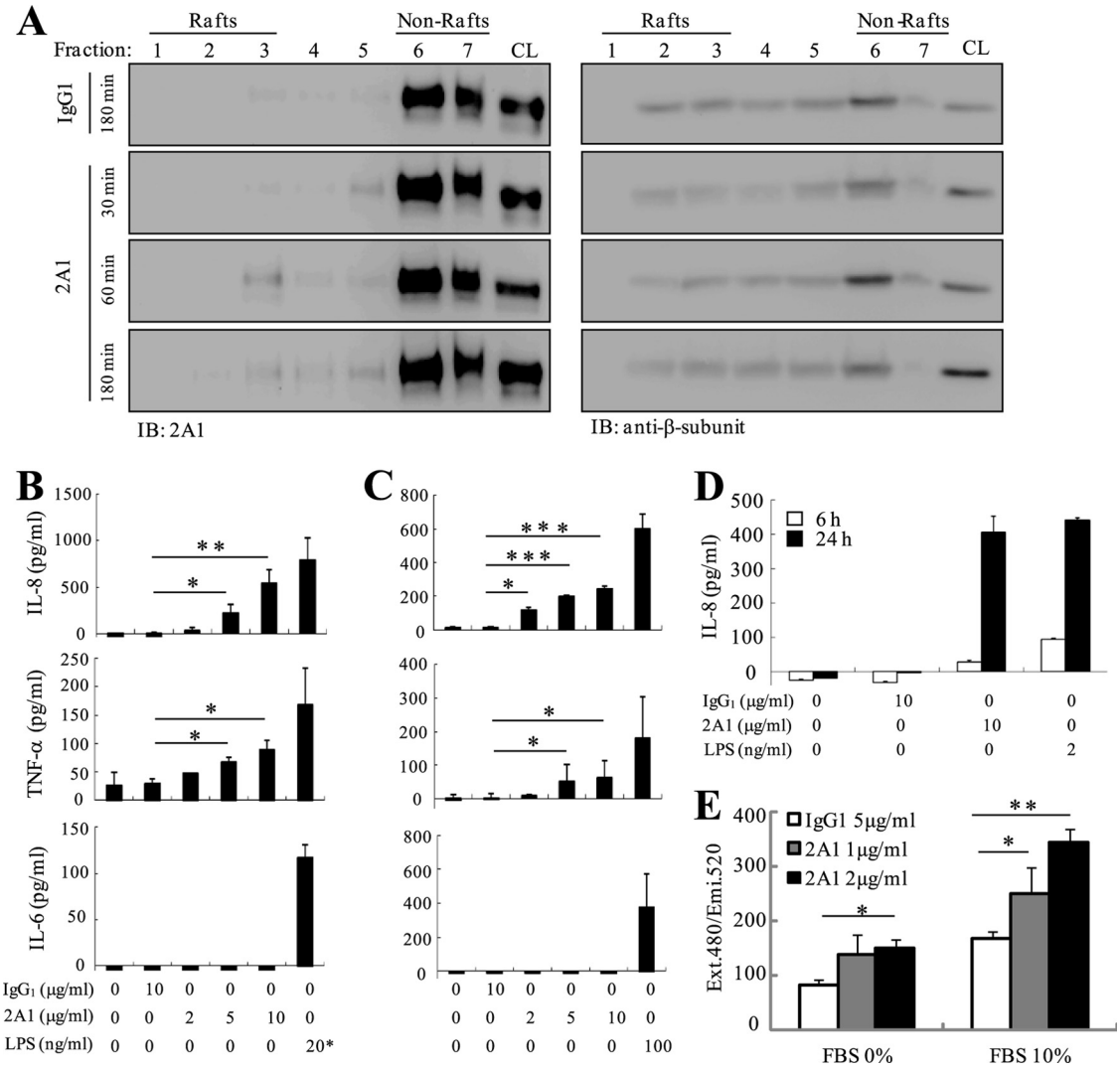

FIG 6 Ligation of EMR2 by immobilized 2A1 MAb induces the translocation of α-subunit to lipid rafts and the production of inflammatory cytokines by macrophages. (A) WB analysis of lipid raft fractions of EMR2(1–5)-WT-expressing stable HT1080 cells stimulated with immobilized 2A1 MAb or isotype control IgG1 for the indicated lengths of time. Distribution patterns of the α-subunit (left panel) and the β-subunit (right panel) in lipid rafts were revealed by probing with 2A1 and rabbit anti-EMR2 β-subunit polyclonal antibodies, respectively. (B and C) ELISA analysis of cytokine production by THP-1 cells (B) and primary human monocytes (C) stimulated with immobilized 2A1 MAb (2, 5, or 10 μg/ml) or isotype control IgG1 (10 μg/ml) for 24 h. LPS was used to treat THP-1 cells (20 ng/ml for IL-8 and TNF-α or 1 μg/ml for IL-6 production) and monocytes (100 pg/ml) as a positive control. (D) ELISA analysis of IL-8 production by THP-1 cells stimulated with immobilized 2A1 MAb (10 μg/ml) or isotype control IgG1 (10 μg/ml) for 6 and 24 h. LPS was used as a positive control. (E) Cell migration analysis of stable HT1080 cells expressing EMR2-WT by stimulation with immobilized 2A1 MAb (1 and 2 μg/ml) or isotype control IgG1 (5 μg/ml) for 3 h. The data are means ± the SEM of three independent experiments performed in triplicate. *, $P < 0.05$; **, $P < 0.01$; ***, $P < 0.005$.

shown) are not produced by 2A1-treated cells, confirming the restricted specificity of immobilized 2A1-induced effect. The possibility of contamination in the system is ruled out since the incubation of soluble 2A1 with THP-1 cells did not induce any cytokine production. These results demonstrate for the first time that sustained ligation of EMR2 α-subunit in macrophages induces the production of specific inflammatory cytokines. Similarly, EMR2 ligation by membrane-coated 2A1 also enhances cell migration of stable HT1080 cells expressing EMR2-WT receptors (Fig. 6E).

Finally, we examined whether the EMR2 β-subunit in lipid rafts is relevant for the 2A1-induced cytokine production. To do this, lipid rafts are disrupted by treating cells with lovastatin or filipin, two commonly used reagents to manipulate the cholesterol levels in cell membranes (41). MβCD, a cholesterol-depleting raft disruptor, causes a high background of cytokine secretion in our macrophage culture system and so was not used further (41). WB analysis revealed effective lipid raft disturbance in lovastatin- and filipin-treated cells, as demonstrated by the apparent changes in the distribution patterns of raft markers such as CD55 (data not shown). Similarly, the localization pattern of EMR2 β-subunit was also shifted more toward the nonraft fractions in treated cells (Fig. 7A and B). Interestingly, when lovastatin- or filipin-treated cells are incubated with immobilized 2A1, the 2A1-induced α-subunit migration to lipid rafts is clearly retarded (Fig. 7A and B). More significantly, the production of IL-8 and TNF-α is reduced dose dependently in lovastatin- and filipin-treated THP-1

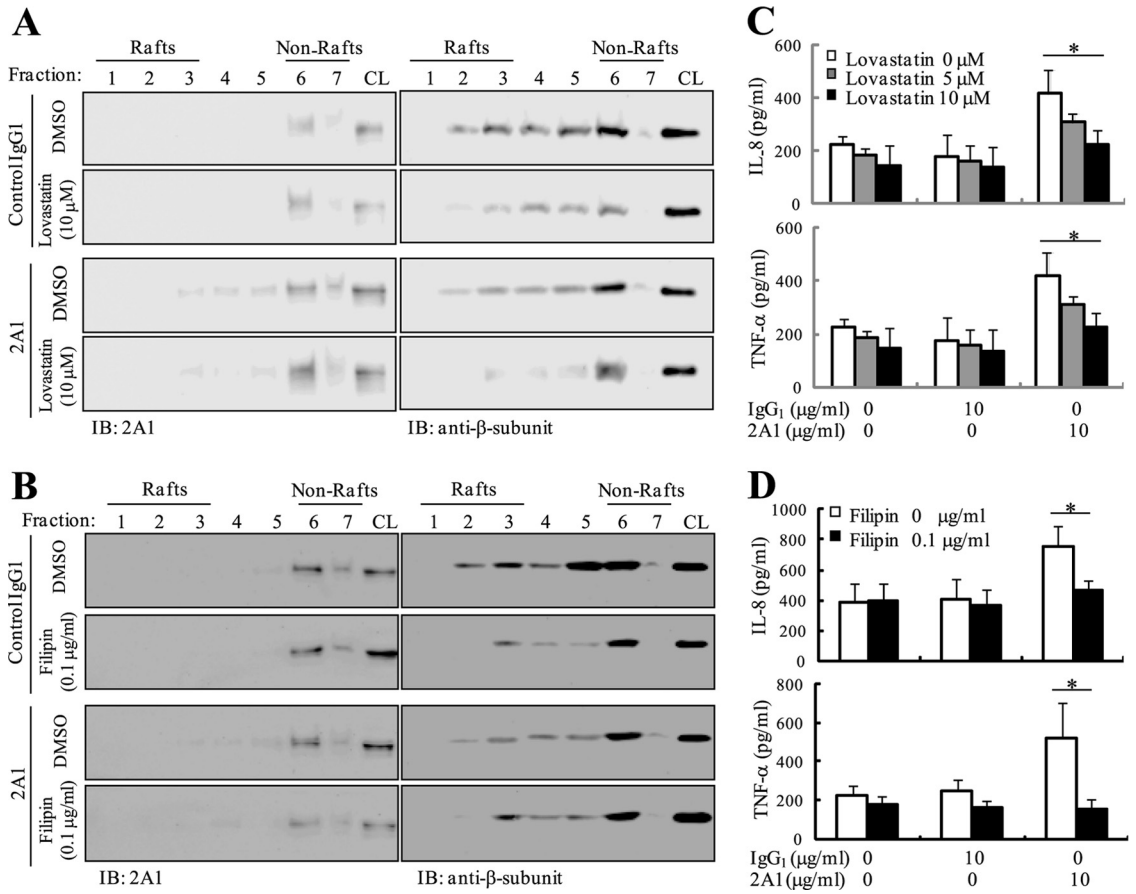

FIG 7 Disruption of lipid rafts reduces 2A1-induced α-subunit translocation and the production of inflammatory cytokines. (A and B) WB analysis of lipid raft fractions of EMR2(1–5)-WT-expressing stable HT1080 cells. Cells were pretreated with (A) lovastatin (10 μM) or with (B) filipin (0.1 μg/ml) and incubated with immobilized 2A1 MAb or control IgG1 for 1.5 h. Dimethyl sulfoxide (DMSO)-treated cells were used as a control. (C and D) THP-1 cells were treated with lovastatin (5 or 10 μM) (C) or filipin (0.1 μg/ml) (D), followed by stimulation with immobilized 2A1 MAb or control IgG1 (10 μg/ml) for 24 h. Supernatant was collected for cytokine ELISA analysis as indicated. The data are means ± the SEM of three independent experiments performed in triplicate. *, $P < 0.05$.

cells (Fig. 7C and D) and primary monocytes (data not shown) upon stimulation by immobilized 2A1. These results indicate that the independent EMR2 β-subunit in lipid rafts is critical for the 2A1-induced translocation of α-subunit to the raft fractions and is most likely responsible for the subsequent production of proinflammatory cytokines.

DISCUSSION

While there is no doubt about the GPS proteolytic modification as an essential step in the biosynthesis of adhesion-GPCRs, its functional role is less well examined. Earlier results suggested that GPS proteolysis is a prerequisite for efficient receptor trafficking to the surface. However, efficient surface expression of GPS cleavage-deficient mutants has been readily detected for other adhesion-GPCRs, indicating additional functional roles for this novel proteolytic modification (28). We have shown previously that GPS cleavage is essential for CD97, an EMR2-related adhesion-GPCR, to induce the upregulation of N-cadherin that promotes homotypic cell-cell aggregation (19). Here, we extend our study by comparing the migratory ability of cells expressing the WT or GPS cleavage-deficient EMR2 (Fig. 1). Our data again clearly demonstrate an essential role for GPS proteolysis in the cellular function of EMR2.

If GPS proteolysis is functionally important, the next obvious question is the relationship between the two resulting receptor subunits and how the receptor function is mediated by them. The idea that the GPS-cleaved α-subunit can self-anchor on the plasma membrane is at first hard to comprehend. However, the various methods used in the present study yielded solid data to confirm the presence of independent α-subunit on the cell membrane (Fig. 2 to 5). The analogy of GPS autoproteolytic reaction and the hydrolysis of Hh proteins also suggested the possibility that the GPS-cleaved α-subunit is modified by a lipid moiety, such as cholesterol in Hh proteins, to facilitate its association with membranes. Surprisingly, results from our EMR2-PAR1 chimeric receptors indicate that GPS autoproteolysis is not required for the membrane-association of α-subunit. This suggests strongly that the potential membrane anchor is located within the stalk region of α-subunit. Alternatively, it is also possible that the α-subunit might interact with an accessory molecule on the cell surface. The molecular identity of the membrane anchor or the accessory molecule requires future identification and characterization.

The next surprise is the finding that a significant portion of the α-subunit is also associated noncovalently with the β-subunit (Fig. 3 to 5). These results indicate the presence of two different receptor complexes as a result of GPS proteolysis: a α-β het-

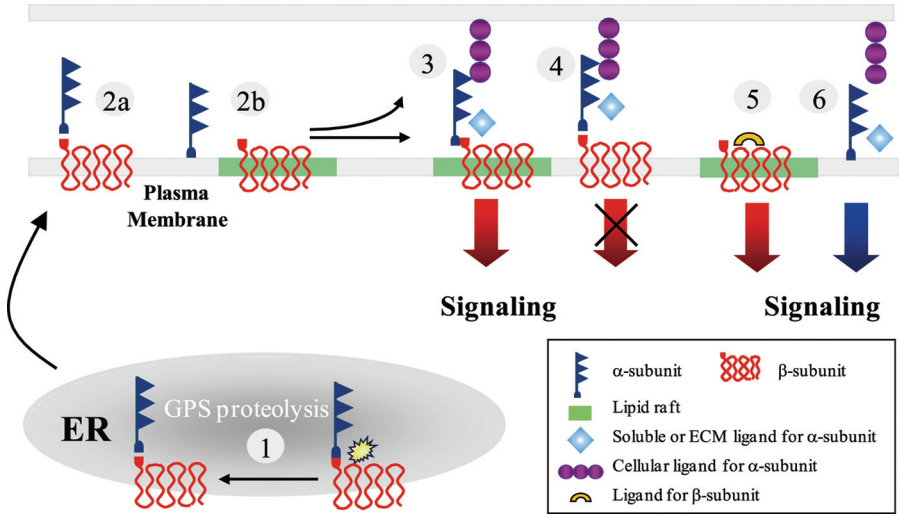

FIG 8 Proposed model of the organization and functional interaction of adhesion-GPCR subunits. (Step 1) the receptor undergoes GPS autoproteolysis in the ER to produce α- and β-subunits. (Step 2) Two distinct forms of receptor complexes are trafficked to the cell membrane: one is the noncovalently linked α-β heterodimer located in the non-lipid raft region (step 2a), and the other consists of the independent α-subunit self-anchored on the non-lipid raft region and the separate β-subunit located in the lipid raft region (green) (step 2b). (Step 3) Upon binding to its cellular or soluble ligand(s) the independent α-subunit is translocated into lipid rafts to reassociate with β-subunit, which activates signaling pathways. (Step 4) Ligand binding to the decoy α-β heterodimeric complex in non-lipid raft regions results in receptor inactivation. (Steps 5 and 6) Alternatively, the independent α- and β-subunits can bind to their respective cognate ligand(s) to induce distinct intracellular signals.

erodimer and independent α- and β-subunits. This conclusion provides excellent explanation for the earlier conflicting results of the latrophilin 1 subunits (38, 40, 48). Nevertheless, it is probably impractical to estimate the ratio of the two receptor complexes since the two are likely to exist in a dynamic equilibrium dependent on the cellular status. In addition, caution should be given to the further interpretation of the data derived from overexpression of chimeric EMR2 molecules. Due to the complex posttranslational modifications of the adhesion-GPCRs, the proportions of incorrectly folded and thus functionally inert proteins might increase in the overexpression system and complicate experimental results.

What is intriguing is the differential distribution of the two independent receptor subunits on membrane raft microdomains and how they regulate receptor function. Similar translocations of leukocyte receptors upon ligand binding have previously been documented. For example, TLR4 transiently moves into lipid raft microdomains after the binding of LPS (46). Upon antibody binding, CD38 on human B cells moves into raft microdomains where it forms a signaling complex with CD19 (14). Raft microdomain partitioning has also been shown to affect the multimerization state of the thyroid stimulating hormone receptor, a member of rhodopsin-family GPCRs (24). However, our data demonstrate for the first time that the translocation and colocalization of two independent receptor subunits derived from a single gene product into lipid rafts results in a cellular response. As such, it demonstrates an entirely new type of signaling mechanism and provides a paradigm for other adhesion-GPCR molecules. Our data also show for the first time that sustained stimulation of the EMR2 α-subunit by immobilized MAb can activate macrophages to secrete specific inflammatory cytokines. The role of raft-associated β-subunit in recruiting α-subunit into lipid rafts and cytokine secretion is further confirmed by the disruption of rafts by lovastatin and filipin. Thus, it seems that the signaling function of EMR2 receptor is mediated mainly by the ligand-induced interaction of "free" α-subunit and "free" β-subunit but not the α-β heterodimer. It is noted here that while we have identified chondroitin sulfate as the cellular ligand of EMR2 previously, 2A1 MAb is used in the present study to provide EMR2-specific ligation and activation as chondroitin sulfate is known to bind to a wide range of cell surface receptors/proteins (42).

The current data summarized above have pointed to several potential outcomes with regard to the conformation and functional interaction of adhesion-GPCR subunits (Fig. 8). Thus, it can be envisioned that, following GPS proteolysis in the endoplasmic reticulum (ER), adhesion-GPCRs are trafficked to the cell surface in two distinct forms of either a closely linked α-β heterodimer or a loose complex of independent α- and β-subunits. While the α-β heterodimer and the independent α-subunit remain mostly in the nonraft regions, the "free" β-subunit is partially localized in the raft fractions. When bound (cross-linked) by its cellular ligand(s) the independent α-subunit is translocated into the raft regions to interact with the "free" β-subunit, which in turn activates signaling pathways. In this model, it is assumed that the raft-excluded α-β heterodimer acts as a decoy receptor. Ligand binding to this heterodimer would result in inactivation, providing an additional level of functional regulation in receptor activity. Nevertheless, it is equally possible that for certain adhesion-GPCRs the binding/ligation of cellular ligands to the α-subunit of the heterodimeric complex might directly induce a signaling event (positive or negative) via the 7TM β-subunit.

Interestingly, recent studies on GPR56 have suggested additional scenarios for the functional interaction of adhesion-GPCR subunits. By making N terminally truncated GPR56, Paavola et al. show that overexpression of GPR56 β-subunit alone results in constitutive receptor activation as well as extensive receptor ubiquitination (33). Likewise, Yang et al. noted a dramatic enhancement of *in vivo* growth and angiogenesis in melanoma cells over-

expressing GPR56 β-subunit, whereas expression of a full-length GPR56 receptor inhibits melanoma angiogenesis (51). These data suggest that the role of GPR56 α-subunit is to interact with and antagonize its constitutive active β-subunit in the steady state. In this scenario, it is notable that we have recently found a distribution pattern for GPR56 subunits in membrane microdomains similar to those of EMR2 (6). In the future, it will be interesting to study the role of lipid rafts in the constitutive activation of GPR56 β-subunit.

Finally, it is also reasonable to hypothesize that the independent α- and β-subunit of some adhesion-GPCRs could possibly bind to their individual cognate ligands and exert their own signaling activities. If this is the case, the "free" β-subunits might be considered as a classical GPCR. Regardless of all of the different potential mechanisms, it is clear that GPS auto-proteolysis and the resulting receptor subunits play an important role in adhesion-GPCR biology. It is hoped that our present report can help shed light on the intriguing relationship between the adhesion-GPCR subunits.

ACKNOWLEDGMENTS

This study was supported by grants from the National Science Council of Taiwan (NSC98-2320-B-182-028-MY3 and NSC96-2320-B-182-005) and Chang Gung Memorial Hospital (CMRPD190551 and CMRPD170143 to H.-H.L. and CMRPG2A0081 to W.-P.T.).

REFERENCES

1. **Anderson KD, et al.** 2011. Angiogenic sprouting into neural tissue requires Gpr124, an orphan G protein-coupled receptor. Proc. Natl. Acad. Sci. U. S. A. **108**:2807–2812.
2. **Bjarnadottir TK, Fredriksson R, Schioth HB.** 2007. The adhesion GPCRs: a unique family of G protein-coupled receptors with important roles in both central and peripheral tissues. Cell. Mol. Life Sci. **64**:2104–2119.
3. **Chang GW, et al.** 2003. Proteolytic cleavage of the EMR2 receptor requires both the extracellular stalk and the GPS motif. FEBS Lett. **547**:145–150.
4. **Chen G, Yang L, Begum S, Xu L.** 2010. GPR56 is essential for testis development and male fertility in mice. Dev. Dyn. **239**:3358–3367.
5. **Chen TY, et al.** EMR2 receptor ligation modulates cytokine secretion profiles and cell survival of lipopolysaccharide-treated neutrophils. Chang Gung Med. J. **34**:468–477.
6. **Chiang NY, et al.** 2011. Disease-associated GPR56 mutations cause bilateral frontoparietal polymicrogyria via multiple mechanisms. J. Biol. Chem. **286**:14215–14225.
7. **Chini B, Parenti M.** 2004. G-protein coupled receptors in lipid rafts and caveolae: how, when and why do they go there? J. Mol. Endocrinol. **32**:325–338.
8. **Cork SM, Van Meir EG.** 2011. Emerging roles for the BAI1 protein family in the regulation of phagocytosis, synaptogenesis, neurovasculature, and tumor development. J. Mol. Med. (Berlin) **89**:743–752.
9. **Coughlin SR.** 2000. Thrombin signaling and protease-activated receptors. Nature **407**:258–264.
10. **Cullen M, et al.** 2011. GPR124, an orphan G protein-coupled receptor, is required for CNS-specific vascularization and establishment of the blood-brain barrier. Proc. Natl. Acad. Sci. U. S. A. **108**:5759–5764.
11. **Das S, et al.** 2011. Brain angiogenesis inhibitor 1 (BAI1) is a pattern recognition receptor that mediates macrophage binding and engulfment of Gram-negative bacteria. Proc. Natl. Acad. Sci. U. S. A. **108**:2136–2141.
12. **Davies B, et al.** 2004. Targeted deletion of the epididymal receptor HE6 results in fluid dysregulation and male infertility. Mol. Cell. Biol. **24**:8642–8648.
13. **Davies JQ, et al.** 2007. The role of receptor oligomerization in modulating the expression and function of leukocyte adhesion-G protein-coupled receptors. J. Biol. Chem. **282**:27343–27353.
14. **Deaglio S, et al.** 2007. CD38/CD19: a lipid raft-dependent signaling complex in human B cells. Blood **109**:5390–5398.
15. **Del Real G, et al.** 2002. Blocking of HIV-1 infection by targeting CD4 to non-raft membrane domains. J. Exp. Med. **196**:293–301.
16. **Devenport D, Oristian D, Heller E, Fuchs E.** 2011. Mitotic internalization of planar cell polarity proteins preserves tissue polarity. Nat. Cell Biol. **13**:893–902.
17. **Galle J, et al.** 2006. Individual cell-based models of tumor-environment interactions: multiple effects of CD97 on tumor invasion. Am. J. Pathol. **169**:1802–1811.
18. **Hoek RM, et al.** 2010. Deletion of either CD55 or CD97 ameliorates arthritis in mouse models. Arthritis Rheum. **62**:1036–1042.
19. **Hsiao CC, Chen HY, Chang GW, Lin HH.** 2011. GPS autoproteolysis is required for CD97 to upregulate the expression of N-cadherin that promotes homotypic cell-cell aggregation. FEBS Lett. **585**:313–318.
20. **Krasnoperov VG, et al.** 1997. alpha-Latrotoxin stimulates exocytosis by the interaction with a neuronal G-protein-coupled receptor. Neuron **18**:925–937.
21. **Kuhnert F, et al.** 2010. Essential regulation of CNS angiogenesis by the orphan G protein-coupled receptor GPR124. Science **330**:985–989.
22. **Kwakkenbos MJ, et al.** 2002. The human EGF-TM7 family member EMR2 is a heterodimeric receptor expressed on myeloid cells. J. Leukoc. Biol. **71**:854–862.
23. **Langenhan T, et al.** 2009. Latrophilin signaling links anterior-posterior tissue polarity and oriented cell divisions in the *Caenorhabditis elegans* embryo. Dev. Cell **17**:494–504.
24. **Latif R, Ando T, Davies TF.** 2007. Lipid rafts are triage centers for multimeric and monomeric thyrotropin receptor regulation. Endocrinology **148**:3164–3175.
25. **Lee JJ, et al.** 1994. Autoproteolysis in hedgehog protein biogenesis. Science **266**:1528–1537.
26. **Lin HH, et al.** 2004. Autocatalytic cleavage of the EMR2 receptor occurs at a conserved G protein-coupled receptor proteolytic site motif. J. Biol. Chem. **279**:31823–31832.
27. **Lin HH, et al.** 2005. The macrophage F4/80 receptor is required for the induction of antigen-specific efferent regulatory T cells in peripheral tolerance. J. Exp. Med. **201**:1615–1625.
28. **Lin HH, Stacey M, Yona S, Chang GW.** 2011. GPS proteolytic cleavage of adhesion-GPCRs. Adv. Exp. Med. Biol. **706**:49–58.
29. **McMillan DR, White PC.** 2011. Studies on the very large g protein-coupled receptor: from initial discovery to determining its role in sensorineural deafness in higher animals. Adv. Exp. Med. Biol. **706**:76–86.
30. **Monk KR, et al.** 2009. A G protein-coupled receptor is essential for Schwann cells to initiate myelination. Science **325**:1402–1405.
31. **Monk KR, Oshima K, Jors S, Heller S, Talbot WS.** 2011. Gpr126 is essential for peripheral nerve development and myelination in mammals. Development **138**:2673–2680.
32. **Ostrom RS, Insel PA.** 2004. The evolving role of lipid rafts and caveolae in G protein-coupled receptor signaling: implications for molecular pharmacology. Br. J. Pharmacol. **143**:235–245.
33. **Paavola KJ, Stephenson JR, Ritter SL, Alter SP, Hall RA.** 2011. The N terminus of the adhesion G protein-coupled receptor GPR56 controls receptor signaling activity. J. Biol. Chem. **286**:28914–28921.
34. **Piao X, et al.** 2004. G protein-coupled receptor-dependent development of human frontal cortex. Science **303**:2033–2036.
35. **Popik W, Alce TM.** 2004. CD4 receptor localized to non-raft membrane microdomains supports HIV-1 entry: identification of a novel raft localization marker in CD4. J. Biol. Chem. **279**:704–712.
36. **Porter JA, et al.** 1995. The product of hedgehog autoproteolytic cleavage active in local and long-range signaling. Nature **374**:363–366.
37. **Qian F, et al.** 2002. Cleavage of polycystin-1 requires the receptor for egg jelly domain and is disrupted by human autosomal-dominant polycystic kidney disease 1-associated mutations. Proc. Natl. Acad. Sci. U. S. A. **99**:16981–16986.
38. **Serova OV, Popova NV, Petrenko AG, Deyev IE.** 2010. Association of the subunits of the calcium-independent receptor of alpha-latrotoxin. Biochem. Biophys. Res. Commun. **402**:658–662.
39. **Shikano S, Li M.** 2003. Membrane receptor trafficking: evidence of proximal and distal zones conferred by two independent endoplasmic reticulum localization signals. Proc. Natl. Acad. Sci. U. S. A. **100**:5783–5788.
40. **Silva JP, Lelianova V, Hopkins C, Volynski KE, Ushkaryov Y.** 2009. Functional cross-interaction of the fragments produced by the cleavage of distinct adhesion G-protein-coupled receptors. J. Biol. Chem. **284**:6495–6506.

41. **Simons K, Toomre D.** 2000. Lipid rafts and signal transduction. Nat. Rev. Mol. Cell Biol. **1**:31–39.
42. **Stacey M, et al.** 2003. The epidermal growth factor-like domains of the human EMR2 receptor mediate cell attachment through chondroitin sulfate glycosaminoglycans. Blood **102**:2916–2924.
43. **Steinert M, et al.** 2002. Expression and regulation of CD97 in colorectal carcinoma cell lines and tumor tissues. Am. J. Pathol. **161**:1657–1667.
44. **Tissir F, et al.** 2010. Lack of cadherins Celsr2 and Celsr3 impairs ependymal ciliogenesis, leading to fatal hydrocephalus. Nat. Neurosci. **13**:700–707.
45. **Trejo J, Altschuler Y, Fu HW, Mostov KE, Coughlin SR.** 2000. Protease-activated receptor-1 down-regulation: a mutant HeLa cell line suggests novel requirements for PAR1 phosphorylation and recruitment to clathrin-coated pits. J. Biol. Chem. **275**:31255–31265.
46. **Triantafilou M, Morath S, Mackie A, Hartung T, Triantafilou K.** 2004. Lateral diffusion of Toll-like receptors reveals that they are transiently confined within lipid rafts on the plasma membrane. J. Cell Sci. **117**:4007–4014.
47. **Veninga H, et al.** 2008. Analysis of CD97 expression and manipulation: antibody treatment but not gene targeting curtails granulocyte migration. J. Immunol. **181**:6574–6583.
48. **Volynski KE, et al.** 2004. Latrophilin fragments behave as independent proteins that associate and signal on binding of LTX(N4C). EMBO J. **23**:4423–4433.
49. **Weston MD, Luijendijk MW, Humphrey KD, Moller C, Kimberling WJ.** 2004. Mutations in the VLGR1 gene implicate G-protein signaling in the pathogenesis of Usher syndrome type II. Am. J. Hum. Genet. **74**:357–366.
50. **Xu L, Begum S, Hearn JD, Hynes RO.** 2006. GPR56, an atypical G protein-coupled receptor, binds tissue transglutaminase, TG2, and inhibits melanoma tumor growth and metastasis. Proc. Natl. Acad. Sci. U. S. A. **103**:9023–9028.
51. **Yang L, et al.** 2011. GPR56 regulates VEGF production and angiogenesis during melanoma progression. Cancer Res. **71**:5558–5568.
52. **Yona S, et al.** 2008. Ligation of the adhesion-GPCR EMR2 regulates human neutrophil function. FASEB J. **22**:741–751.
53. **Yona S, Lin HH, Siu WO, Gordon S, Stacey M.** 2008. Adhesion-GPCRs: emerging roles for novel receptors. Trends Biochem. Sci. **33**:491–500.
54. **Yoneyama A, Nakahara K, Higashihara M, Kurokawa K.** 1995. Increased levels of soluble CD8 and CD4 in patients with infectious mononucleosis. Br. J. Haematol. **89**:47–54.